Reprinted from JOURNAL OF CLIMATE AND APPLIED METEOROLOGY, Vol. 23, No. 7, July 1984
American Meteorological Society
Printed in U.S.A.

A Model of the Radiative Properties of the El Chichon Stratospheric Aerosol Layer

MICHAEL D. KING, HARSHVARDHAN[1] AND ALBERT ARKING

Laboratory for Atmospheric Sciences, Goddard Space Flight Center, NASA, Greenbelt, MD 20771

(Manuscript received 2 December 1983, in final form 1 May 1984)

ABSTRACT

An accurate multiple-scattering model has been employed to examine the effect of an aerosol layer at 25 mb, corresponding to the El Chichon observations, on the reflection, transmission and absorption of radiation by the stratosphere as a function of latitude, optical thickness and aerosol size distribution. Results are presented and parameterized for each of two wavelength intervals in the shortwave region and 17 wavelength intervals in the longwave region for three models of the aerosol size distribution. They include one model representing the unperturbed stratospheric aerosol plus two models based on measurements of the El Chichon aerosol size distribution. In addition to models of the radiative properties of the aerosol layer, a simple model of the latitudinal distribution of aerosol optical thickness as a function of time is developed, based on diffusive transport in latitude and exponential decay in time. These parameterizations for solar and infrared radiation, together with the dispersion model, permit climate models to account for the evolution of an aerosol size distribution from post-volcanic conditions to background conditions.

1. Introduction

Throughout history the earth has experienced periodic volcanic eruptions of sufficient magnitude to substantially increase the aerosol optical thickness of the stratosphere for a couple of years, primarily through chemical transformation and condensation of SO_2 injected directly into the stratosphere (Turco *et al.*, 1982). The eruptions of El Chichon in Chiapas, Mexico from 28 March to 4 April 1982 created an aerosol layer with the largest optical thickness ever recorded at Mauna Loa Observatory in the 25-year history of observations (Mitchell, 1982). This is in part due to the unique location of Mauna Loa at a latitude near that of El Chichon (17.3°N), and in part due to the high sulfur content of the El Chichon magma which resulted in a large injection of SO_2 gas into the stratosphere (Krueger, 1983).

The role of stratospheric aerosols in modifying the energy budget of the earth–atmosphere–ocean system has been the subject of numerous theoretical investigations in recent years. Pollack *et al.* (1976) used a globally averaged radiative–convective model with a fixed temperature lapse rate to examine the change in the spherical albedo of the earth–atmosphere system as a function of the change in stratospheric optical thickness. Since Pollack *et al.* assumed the aerosol size distribution following a volcanic eruption is the same as that for background, unperturbed conditions, potentially important radiative effects resulting from the temporal evolution of the aerosol size distribution were neglected. Furthermore, the aerosol layer from a single eruption spreads over the earth such that the aerosol optical thickness is a function of space and time. In spite of these limitations, Pollack *et al.* (1976) made the earliest steady-state estimate of the change in surface and stratospheric temperatures following major volcanic eruptions.

Herman *et al.* (1976), Harshvardhan (1979) and Lenoble *et al.* (1982) have examined the radiative effects of a stratospheric aerosol layer when the tropospheric albedo and solar zenith angle are allowed to vary with latitude and season. In addition, Harshvardhan and Lenoble *et al.* considered the partially compensating influence of terrestrial radiation, confirming the earlier findings of Harshvardhan and Cess (1976) and Pollack *et al.* (1976) that the dominant effect of volcanic aerosols on the earth's radiation budget is an increase in the reflection of solar radiation, with only a modest reduction in the emission of terrestrial radiation to space.

In the aftermath of the El Chichon eruptions, the stratospheric aerosol layer has been subject to extensive observations from a variety of platforms. Airborne active and passive sensors have provided unprecedented detail on the horizontal and vertical distribution of the aerosol layer (McCormick and Swissler, 1983; Spinhirne, 1983; Swissler *et al.*, 1983). Information on particle size was obtained by inverting spectral solar transmission measurements obtained at Mauna Loa Observatory (DeLuisi *et al.*, 1983) as will be described below. *In situ* measurements with bal-

[1] Also affiliated with: Department of Meteorology, University of Maryland, College Park, MD 20742.

loon-borne particle counters (Hofmann and Rosen, 1983a,b) have also provided particle size distributions as well as information on composition. These measurements provide a fairly comprehensive, although tentative, picture of the nature and spatial distribution of the stratospheric aerosol layer following the El Chichon eruptions. Of course, many puzzling aspects of the data collected so far are yet to be explained. But it is worthwhile at this point to synthesize the information we now have into a radiative model of the aerosol layer that could be used to determine its effect on the radiation field of the earth–atmosphere system. This paper will concentrate on the radiative properties of the aerosol layer, the results of which can be utilized as input to climate models for climate sensitivity studies.

The present study examines the radiative properties of an aerosol layer at 25 mb as a function of latitude, optical thickness and size distribution, where the aerosol particles are assumed to consist of a 75% H_2SO_4 (by weight) aqueous solution. Our multiple-scattering computations were performed for each of 15 wavelengths in the shortwave spectral region by successive applications of the invariant imbedding and doubling methods with polarization neglected (King, 1983). Results are presented and parameterized for each of two broadband wavelength intervals and for three models of the aerosol size distribution. For the longwave region we obtained the global transmission (flux transmissivity) for 17 broadband wavelength intervals using the single scattering approximation to account for the small, though nonnegligible, scattering component of the aerosols at infrared wavelengths. Two of the size distribution models are based on measurements of the El Chichon aerosol layer, while the third model is representative of background, unperturbed conditions. We also develop a simple model of the spatial and temporal distribution of the aerosol layer, based on diffusive transport in latitude and exponential decay in time. These parameterizations for solar and infrared radiation, together with our dispersion model, are ideally suited to studying the sensitivity of climate to stratospheric aerosol perturbations using a multi-layer energy balance climate model in an annually and zonally averaged form (Peng *et al.*, 1982).

2. Optical properties of the aerosol layer

Crucial to our ability to calculate the radiative effects of the El Chichon stratospheric aerosol layer is a knowledge of the aerosol microphysical model. The microphysical model requires specification of the composition, shape and size distribution of the particles. Since the long-lived sulfate aerosols in the stratosphere are primarily formed by chemical transformation and condensation of SO_2 injected there by volcanic eruptions (Turco *et al.*, 1982), it is now fairly well established that the particles are primarily spherical liquid droplets having a 75% concentration by weight of sulfuric acid (Rosen, 1971). The El Chichon aerosol layer appears to be no exception, with recent balloon-borne boiling point measurements indicating that, on average, the stratospheric aerosol layer is composed of a 75% H_2SO_4 aqueous solution (Hofmann and Rosen, 1983a). Information on the size distribution of the particles in the El Chichon layer was particularly lacking in the early months following the eruptions because the height of the layer (~25 km, 25 mb) made it inaccessible to instrumented aircraft.

a. Aerosol size distributions

One of the methods which has been adopted for estimating the aerosol size distribution of the El Chichon layer is the constrained linear inversion method described by King (1982). In this method, the columnar aerosol size distribution is inferred by numerically inverting aerosol optical depth measurements as a function of wavelength. Utilizing atmospheric transmission measurements collected at Mauna Loa Observatory in five wavelength bands between 0.38 and 1.06 μm, the monthly mean stratospheric aerosol optical depths have been determined for July 1982 (DeLuisi *et al.*, 1983). These results, obtained by subtracting the molecular scattering, ozone absorption and estimated background tropospheric aerosol contributions from the total optical depth, are presented in the left portion of Fig. 1. The standard deviations of the optical thickness measurements about the mean are also presented. At this time and location, the stratospheric aerosol layer had an optical depth between 0.15 and 0.25 throughout the visible wavelength region. This is more than an order of magnitude larger than background levels of the total aerosol optical depth at Mauna Loa (Shaw, 1979).

The columnar aerosol size distribution obtained by inverting the Mauna Loa measurements is presented in the right portion of Fig. 1, while the solid curve in the left portion indicates how the inverted size distribution reproduces the aerosol optical thickness measurements. Due to the prominent negative curvature in the spectral optical thickness measurements, the corresponding size distribution is quite narrow with a peak concentration at radii between 0.3 and 0.4 μm. Though the inversion was performed assuming the complex refractive index of the aerosol particles was wavelength and size independent and given by $m = 1.45 - 0.00i$, it is well-known that the refractive index sensitivity is quite weak, affecting the inverted size distribution slightly by shifting its magnitude and radii while maintaining its overall shape (King *et al.*, 1978).

The columnar size distribution presented in Fig. 1, representing the number of particles per square cm

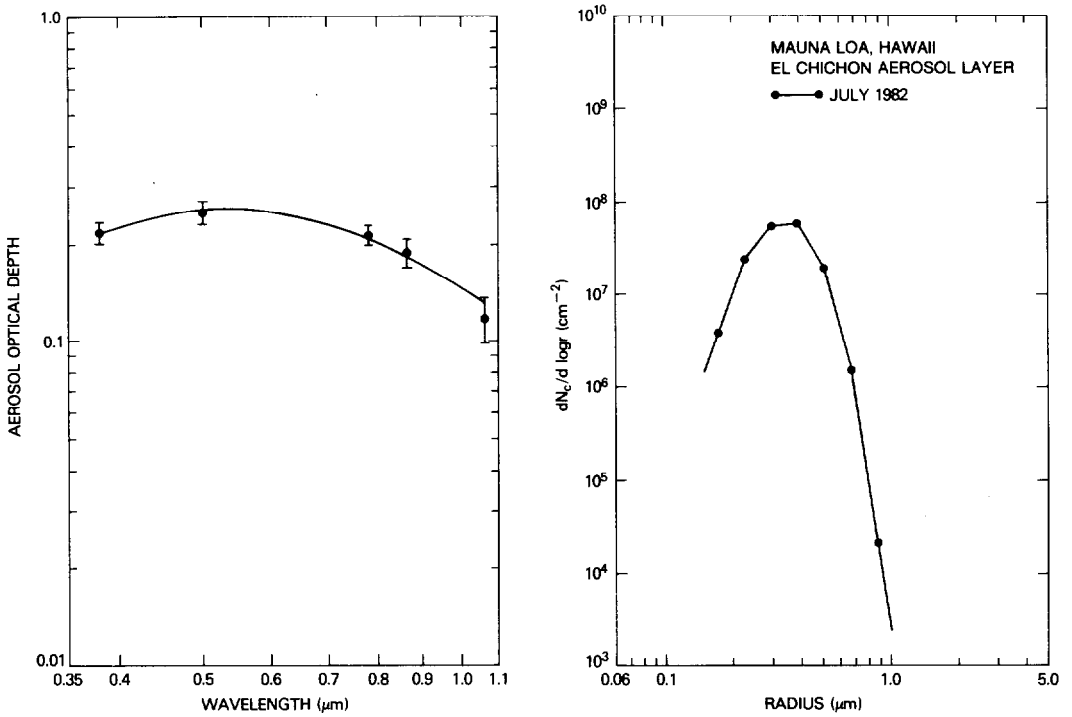

FIG. 1. Monthly mean stratospheric aerosol optical thickness and estimated size distribution for measurements collected at Mauna Loa Observatory during July 1982. The curve on the left indicates the regression fit to the data using the inverted size distribution.

per log radius interval in a vertical column through the stratosphere, is well described by a modified gamma distribution of the form

$$\frac{dN_c}{d\log r} = Cr^{\nu+1}\exp(-\beta r), \tag{1}$$

where the mode radius $r_0 = (\nu + 1)/\beta$. The distribution presented in Fig. 1 was fit to (1) using an efficient gradient-expansion method from nonlinear least-squares theory (Bevington, 1969, 232–242). The coefficients yielding the best fit to the Mauna Loa distribution were found to be $C = 9.897 \times 10^{19}$ cm^{-2} μm$^{-13.65}$, $\nu = 12.65$, $\beta = 39.3$ μm^{-1} and $r_0 = 0.35$ μm. For a particle density of 1.65 g cm^{-3}, corresponding to spherical droplets having a 75% concentration by weight of sulfuric acid, the Mauna Loa distribution implies a columnar mass loading of 66 mg m^{-2}.

As an alternative estimate of the size distribution of the stabilized El Chichon stratospheric aerosol layer, we used balloon-borne particle counter measurements made by Hofmann and Rosen (1983a) at Del Rio, Texas (29.2°N) on 23 October 1982. These measurements were obtained through the use of a complement of three optical particle counters to determine the number of particles having radii greater than 0.01, 0.15, 0.25, 0.95, 1.2 and 1.8 μm. These particle counter systems have been described by Hofmann and Rosen (1982). The aerosol size distribution for the column is obtained by integrating the cumulative size distributions between 21.5 and 24.5 km, corresponding to the altitude range containing the dominant aerosol concentration. Following Hofmann and Rosen (1983b), the balloon-borne observations are described in terms of a bimodal log-normal distribution of the form

$$\frac{dN_c}{d\log r} = \sum_{l=1}^{2}\frac{C_l}{\sigma_l}\exp[-(\ln r - \ln r_l)^2/(2\sigma_l^2)]. \tag{2}$$

In this expression r_l is the mode radius, σ_l the natural logarithm of the geometric standard deviation and C_l a constant which determines the total particulate number density of the lth mode. Scaling the observations such that the optical thickness at 0.55 μm is the same as that for the Mauna Loa observations, we find that $C_1 = 50C_2$, $r_1 = 0.27$ μm, $\sigma_1 = \ln 1.5$, $C_2 = 3.869 \times 10^5$ cm^{-2}, $r_2 = 1.0$ μm and $\sigma_2 = \ln 1.1$. In contrast to the Mauna Loa size distribution, this distribution implies a total columnar mass loading of 90 mg m^{-2}, of which 30 mg m^{-2} is due to the large particle mode ($l = 2$).

Figure 2 illustrates the columnar aerosol size distributions for the Mauna Loa and Hofmann and Rosen (1983b) estimates of the El Chichon stratospheric aerosol layer. In addition, the Standard Radiation Atmosphere model representing unperturbed background conditions is presented (McClatchey *et*

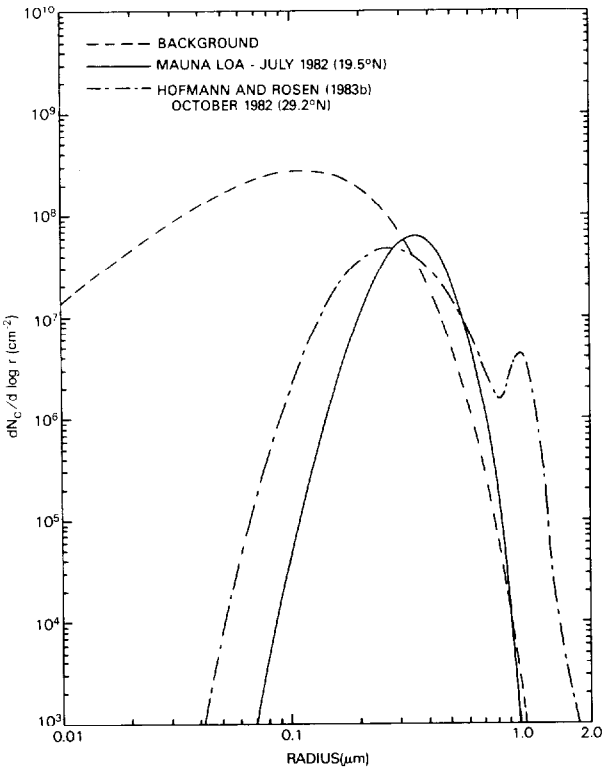

FIG. 2. Columnar aerosol size distributions for three models of the stratospheric aerosol. The background size distribution represents the unperturbed stratospheric aerosol, whereas the Mauna Loa and Hofmann and Rosen (1983b) distributions are derived from measurements of the El Chichon stratospheric aerosol layer during July and October 1982, respectively. All distributions are normalized to yield the same aerosol optical thickness at $\lambda = 0.55$ μm.

al., 1980), where we have scaled the magnitude of this distribution to yield the same aerosol optical thickness as the two El Chichon models at a reference wavelength of 0.55 μm. This background distribution is a modified gamma distribution [Eq. (1)] having coefficients $C = 1.674 \times 10^{11}$ cm^{-2} μm^{-2}, $\nu = 1$ and $\beta = 18$ μm^{-1}, from which we find $r_0 = 0.11$ μm and a columnar mass loading of 64 mg m^{-2}.

b. Spectral properties

In addition to the columnar mass loading, each of the aerosol size distribution models has been used to determine the optical thickness, single scattering albedo and asymmetry factor as a function of wavelength between 0.25 and 25.0 μm. These results, presented in Figs. 3–5, are based on the aerosol particles being spherical droplets composed of a 75% (by weight) H_2SO_4 aqueous solution having the complex refractive indices tabulated by Palmer and Williams (1975). Due primarily to the 1.0 μm mode in the Hofmann and Rosen (1983b) distribution, the optical thickness, single scattering albedo and asymmetry factor are noticeably enhanced over results for the other two models in the near and thermal infrared regions. The implication of these differences on the radiative properties of the stratospheric aerosol layer will be discussed in the following sections.

3. Radiative properties of the aerosol layer

A complete description of the radiative properties of the aerosol layer is provided by the reflection and transmission functions at the top and bottom boundaries of the layer, which are, in turn, functions of wavelength and direction. To imbed this layer into a model earth–atmosphere system requires a knowledge of the corresponding functions at the levels of the model that interface with the aerosol layer. Although the adding–doubling method (Hansen and Travis, 1974; van de Hulst, 1980) can be utilized to combine these functions and derive flux and heating rate profiles within the atmosphere, the radiation parameterization in the vast majority of climate models is not sufficiently detailed to utilize the information in this form. We have therefore adopted a more practical approach in which the spectrum was divided into a shortwave region, appropriate for solar radiation and where scattering is an important process, and a

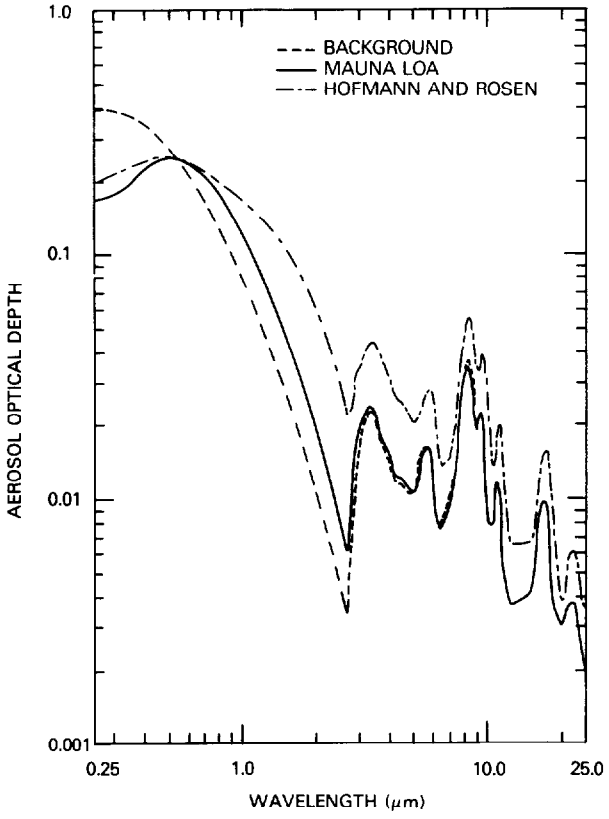

FIG. 3. Aerosol optical thickness as a function of wavelength for the three stratospheric aerosol size distributions presented in Fig. 2, where the aerosol particles are assumed to be composed of a 75% H_2SO_4 aqueous solution.

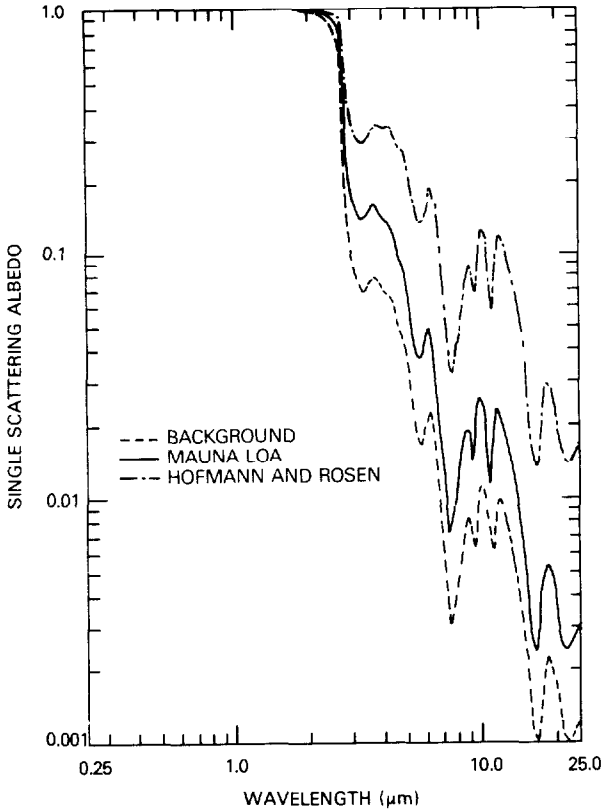

FIG. 4. As in Fig. 3 except for the single scattering albedo of the aerosol particles.

longwave region, appropriate for thermally emitted radiation and where absorption is the dominant process. In the shortwave region a radiative model of the stratosphere was developed, with the aerosol layer imbedded in it. Reflection and transmission functions were calculated in that case for the stratosphere as a whole, appropriately integrated over selected wavelength intervals and angle ranges to meet climate model requirements. In the longwave region it was possible to treat the aerosol layer as if it were a purely absorbing medium, with the effects of scattering incorporated into an effective optical thickness. In that case it was sufficient to calculate the transmission and reflection functions of the aerosol layer alone. The target model for these calculations is the multilayer energy balance model developed by Peng *et al.* (1982). The resulting functions, however, can be utilized in a wide range of climate models by combining them to meet the model requirements and appropriately incorporating them into the model's radiation parameterization schemes.

a. Shortwave radiation

The shortwave portion of the spectrum is divided into two regions: 1) $\lambda \leq 0.83$ μm, where water vapor and aerosol absorption are negligible but ozone absorption is significant and 2) $\lambda > 0.83$ μm where ozone absorption is negligible but aerosol absorption is important in the stratosphere and water vapor absorption is important in the troposphere. The stratosphere is assumed to be divided into three sublayers, two of which contain ozone and one of which contains the aerosol particles (see Fig. 6). The ozone content of each sublayer, denoted Ω_1 above and Ω_2 below the aerosol layer, is a function of latitude as well as the altitude assumed for the aerosol layer. The values of Ω_1 and Ω_2 used in the present investigation are presented in Table 1. These values, which were determined for annually averaged conditions using the model atmospheres of McClatchey *et al.* (1972), assume the tropopause is located at 200 mb and the aerosol layer is located at 25 mb (~25 km). This altitude of the aerosol layer is compatible with lidar observations during the first 6 months following the eruptions of El Chichon (Coulson, 1983; DeLuisi *et al.*, 1983).

Radiative transfer computations have been performed for each microphysical model and for 15 wavelength intervals λ_i (six in the region $\lambda \leq 0.83$ μm and nine in the region $\lambda > 0.83$ μm). The method

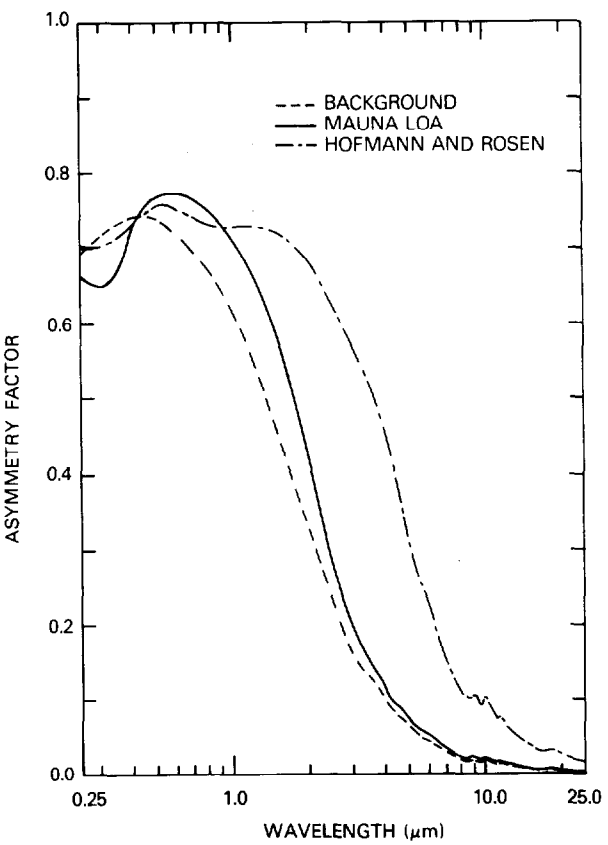

FIG. 5. As in Fig. 3 except for the asymmetry factor of the aerosol particles.

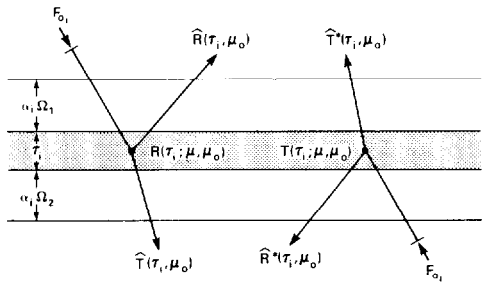

FIG. 6. Schematic illustration of the reflection and transmission of radiation by the stratosphere illuminated by collimated radiation from above (left) and from below (right). Dots denote scattering and absorption events which take place within the aerosol layer of optical thickness τ_i. Both above and below the aerosol layer, the stratosphere is assumed to consist of ozone layers having optical thicknesses $\alpha_i\Omega_1$ and $\alpha_i\Omega_2$, respectively, where Ω_1 and Ω_2 represent the ozone contents of the ozone layers.

used to calculate the diffuse radiation field is the doubling method described by Hansen and Travis (1974), where it was necessary to consider only azimuth-independent radiation. In this method, the reflection and transmission functions of a single layer of optical thickness $\tau_i/2$ are combined with those of a similar layer to obtain the reflection and transmission functions of the combined layer of optical thickness τ_i. The reflection and transmission functions of the initial layer of infinitesimal optical thickness were obtained using the invariant imbedding initialization described by King (1983).

In terms of the azimuth-independent reflection function $R(\tau_i; \mu, \mu_0)$, the albedo of the aerosol layer of optical thickness τ_i is given by

$$\hat{R}(\tau_i, \mu_0) = 2\int_0^1 R(\tau_i; \mu, \mu_0)\mu d\mu.$$

In this expression μ_0 is the cosine of the solar zenith angle and μ the cosine of the zenith angle with respect to the outward normal ($0 \leqslant \mu, \mu_0 \leqslant 1$). Due to the presence of ozone above and below the aerosol layer, the albedo for collimated radiation from above the stratosphere $[\hat{R}(\tau_i, \mu_0)]$ differs from the albedo for collimated radiation from below $[\hat{R}^*(\tau_i, \mu_0)]$. If we let α_i denote the ozone absorption coefficient such that $\alpha_i\Omega_1$ and $\alpha_i\Omega_2$ are the ozone optical depths of the two ozone sublayers (cf. Fig. 6), it follows that

$$\hat{R}(\tau_i, \mu_0) = 2e^{-\alpha_i\Omega_1/\mu_0}\int_0^1 R(\tau_i; \mu, \mu_0)e^{-\alpha_i\Omega_1/\mu}\mu d\mu, \quad (3)$$

$$\hat{R}^*(\tau_i, \mu_0) = 2e^{-\alpha_i\Omega_2/\mu_0}\int_0^1 R(\tau_i; \mu, \mu_0)e^{-\alpha_i\Omega_2/\mu}\mu d\mu. \quad (4)$$

The reflection function of the aerosol layer was computed at each of 15 wavelength intervals using the monochromatic optical properties illustrated in Figs. 3 and 4, together with all coefficients of the Legendre polynomial expansion of the phase function. For the wavelength region $\lambda \leqslant 0.83$ μm it was necessary to further subdivide the spectrum in order to account for the large spectral variation of the ozone absorption coefficients. The reflection function at a wavelength resolution of 0.01 μm was estimated by interpolating from computations performed at 0.25, 0.35, 0.45, 0.55, 0.65 and 0.8 μm. This is a good approximation, since the aerosol optical properties vary slowly with wavelength while the ozone absorption coefficients are more rapidly varying.

The ozone absorption coefficients used for the visible wavelength region were those tabulated by Ackerman (1971). They represent a composite of measurement results reported by other observers. For the ultraviolet region, where the ozone cross sections have a significant temperature dependence, we used Vigroux's (1953) measurements at 229 K for $\lambda > 0.30$ μm and Inn and Tanaka's (1953) measurements at 291 K for $\lambda \leqslant 0.30$ μm, where the latter data were adjusted to a temperature of 229 K using Vigroux's (1953) measurements of the temperature dependence of the ozone cross sections. In the Huggins bands, where the temperature dependence is especially significant, differences as large as 25% occur between these results and those tabulated by Ackerman (1971). In the Chappuis band of the visible wavelength region, the ozone absorption cross sections have no resolvable temperature dependence (Penny, 1979).

The albedo for each microphysical model was integrated over each spectral region, weighted by the spectral solar irradiance F_{0_i}. The spectrally averaged albedo was obtained as a function of latitude (ϕ) and stratospheric aerosol optical thickness at a reference wavelength of 0.55 μm [$\tau_{\text{ref}} = \tau$ (0.55 μm)], where we used the annual mean solar zenith angle and ozone contents presented in Table 1. Fig. 7 illustrates these results for solar illumination from above the stratosphere in five different latitude zones. For the region $\lambda \leqslant 0.83$ μm, shown on the left, the background model has a larger albedo than either of the two El Chichon models. This is primarily a consequence of the larger aerosol optical thickness at wavelengths

TABLE 1. Annual mean cosine of the solar zenith angle (μ_0) and values of the ozone content above (Ω_1) and below (Ω_2) the stratospheric aerosol layer as a function of latitude. The tropopause is located at 200 mb and the aerosol layer at 25 mb.

Latitude (°N)	μ_0	Ω_1 (m atm-cm)	Ω_2 (m atm-cm)
85	0.257	101	249
75	0.274	101	249
65	0.316	104	229
55	0.385	108	209
45	0.453	111	189
35	0.513	115	156
25	0.560	119	123
15	0.592	124	90
5	0.609	124	90

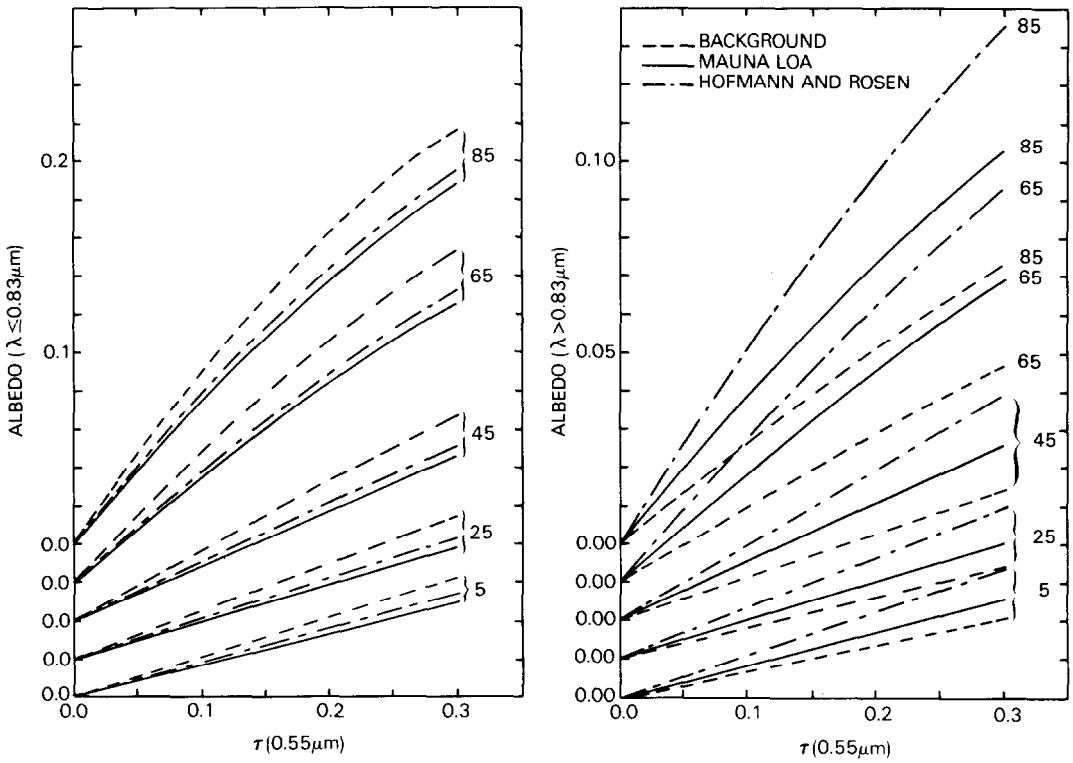

FIG. 7. Diffuse reflection (albedo) as a function of stratospheric aerosol optical thickness at $\lambda = 0.55$ μm for the three aerosol size distributions presented in Fig. 2 and for the annual mean solar zenith angle in five different latitude zones. The figure on the left applies to $\lambda \leq 0.83$ μm and the figure on the right to $\lambda > 0.83$ μm.

less than 0.55 μm (cf. Fig. 3). For the region $\lambda > 0.83$ μm, on the other hand, the El Chichon models have a larger albedo than the background model due to the presence of larger particles. The near-infrared albedo for the Hofmann and Rosen (1983b) model is especially enhanced over that for either of the other two models due to the presence of the 1.0 μm mode in the Hofmann and Rosen size distribution.

As in the case of diffuse reflection (albedo), the diffuse transmission for collimated radiation from above the stratosphere $[\hat{T}(\tau_i, \mu_0)]$ differs from the diffuse transmission for collimated radiation from below $[\hat{T}^*(\tau_i, \mu_0)]$. They are related to the azimuth-independent transmission function of the aerosol layer $T(\tau_i; \mu, \mu_0)$ as follows,

$$\hat{T}(\tau_i, \mu_0) = 2e^{-\alpha_i\Omega_1/\mu_0} \int_0^1 T(\tau_i; \mu, \mu_0) e^{-\alpha_i\Omega_2/\mu} \mu d\mu, \quad (5)$$

$$\hat{T}^*(\tau_i, \mu_0) = 2e^{-\alpha_i\Omega_2/\mu_0} \int_0^1 T(\tau_i; \mu, \mu_0) e^{-\alpha_i\Omega_1/\mu} \mu d\mu. \quad (6)$$

The spectrally averaged diffuse transmission for solar illumination from above the stratosphere is presented in Fig. 8. For $\lambda \leq 0.83$ μm the diffuse transmission is virtually identical for each microphysical model, whereas for $\lambda > 0.83$ μm large differences arise between the models. On comparison with Fig. 7, we find that the Hofmann and Rosen (1983b) model has not only a larger albedo but also a larger diffuse transmission than the other two models in the near-infrared. This is, of course, due to a larger optical thickness, asymmetry factor and single scattering albedo than the Mauna Loa and background models, all of which are a consequence of the larger particles in the Hofmann and Rosen model.

In terms of the diffuse reflection and transmission of collimated radiation, it follows that the fractional absorption of solar radiation for collimated radiation from above $[A(\tau_i, \mu_0)]$ and from below $[A^*(\tau_i, \mu_0)]$ the stratosphere is given, respectively, by

$$A(\tau_i, \mu_0) = 1 - \hat{R}(\tau_i, \mu_0) - \hat{T}(\tau_i, \mu_0) - D(\tau_i, \mu_0), \quad (7)$$

$$A^*(\tau_i, \mu_0) = 1 - \hat{R}^*(\tau_i, \mu_0) - \hat{T}^*(\tau_i, \mu_0) - D(\tau_i, \mu_0). \quad (8)$$

In these expressions the direct transmission $D(\tau_i, \mu_0)$ is given by

$$D(\tau_i, \mu_0) = \exp[-(\alpha_i\Omega_1 + \tau_i + \alpha_i\Omega_2)/\mu_0]. \quad (9)$$

Figure 9 illustrates the spectrally averaged absorption for solar illumination from above the stratosphere. For the region $\lambda > 0.83$ μm, where ozone absorption is negligible, the Hofmann and Rosen (1983b) model absorbs more solar radiation than the other two

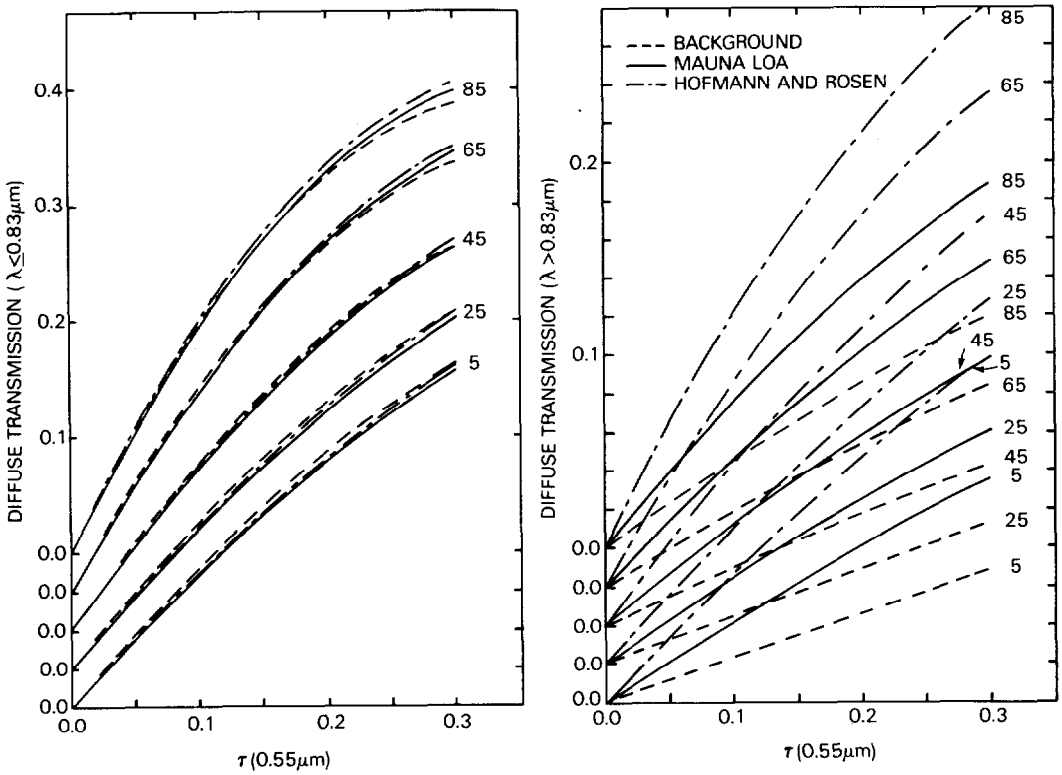

FIG. 8. As in Fig. 7 except for diffuse transmission.

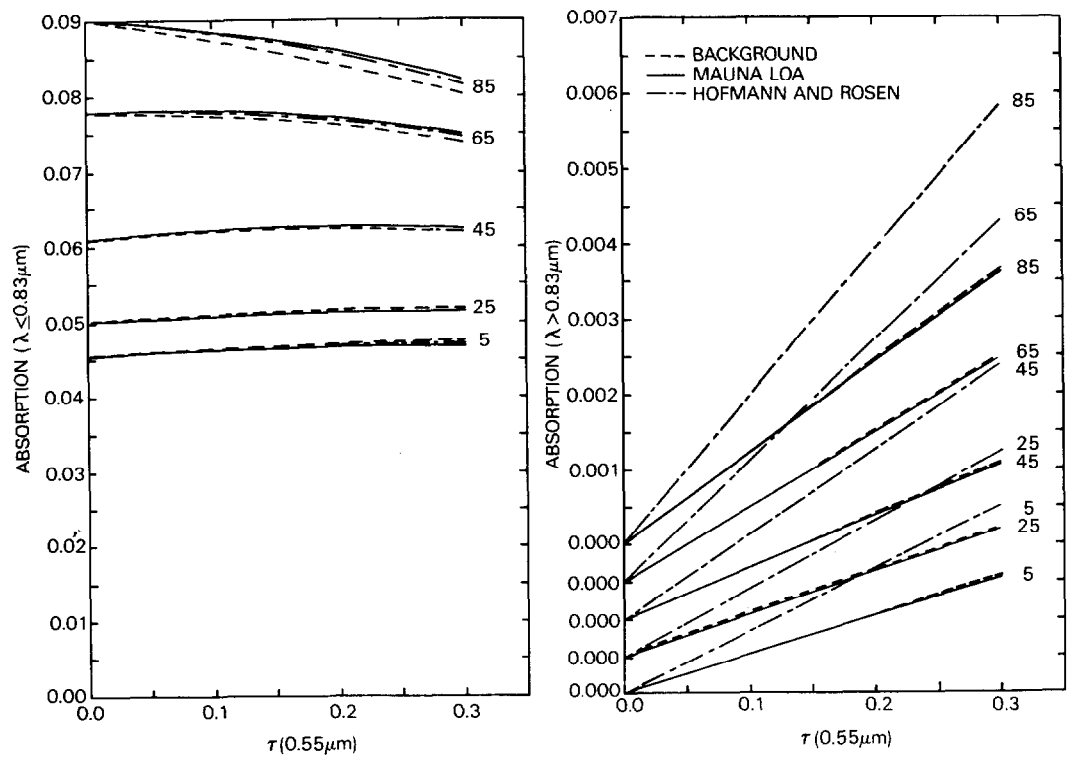

FIG. 9. As in Fig. 7 except for fractional absorption.

models. Although the Hofmann and Rosen model has a larger single scattering albedo than the Mauna Loa and background models, the larger optical thickness more than compensates for the small single scattering absorption such that the overall absorption is enhanced. For the Mauna Loa and background models, the slightly greater optical thickness of the Mauna Loa model is offset by the slightly smaller single scattering absorption. As a consequence, the Mauna Loa and background models have nearly the same spectrally averaged absorption in the near-infrared. For $\lambda \leq 0.83$ μm, where aerosol absorption is negligible but ozone absorption is significant, the absorption has relatively little dependence on either the microphysical model or the aerosol optical thickness. Only for the higher latitudes, where the mean annual solar zenith angle is large, does the absorption have any appreciable sensitivity to τ_{ref}.

In order to compute the radiative flux densities at the top and bottom boundaries of the stratosphere, as well as at the boundaries of all layers comprising the troposphere, it is necessary to determine the radiative properties of the stratosphere for diffuse radiation from below. For many practical purposes it is sufficient to approximate the diffuse radiation from below as isotropic, in which case it is necessary to calculate the spherical (global) albedo, global diffuse transmission, global direct transmission and global absorption:

$$\bar{R}^*(\tau_i) = 2\int_0^1 \hat{R}^*(\tau_i, \mu_0)\mu_0 d\mu_0, \quad (10)$$

$$\bar{T}^*(\tau_i) = 2\int_0^1 \hat{T}^*(\tau_i, \mu_0)\mu_0 d\mu_0, \quad (11)$$

$$\bar{D}(\tau_i) = 2\int_0^1 D(\tau_i, \mu_0)\mu_0 d\mu_0$$

$$= 2E_3(\alpha_i\Omega_1 + \tau_i + \alpha_i\Omega_2), \quad (12)$$

$$\bar{A}^*(\tau_i) = 1 - \bar{R}^*(\tau_i) - \bar{T}^*(\tau_i) - \bar{D}(\tau_i), \quad (13)$$

where $E_3(x)$ is the exponential integral. In addition to the explicit dependence of these functions on optical thickness τ_i, there is an implicit dependence on latitude for the wavelength interval $\lambda \leq 0.83$ μm. This arises from the latitudinal variation of Ω_1 and Ω_2.

If one makes the approximation that the diffuse radiation is isotropic over the hemisphere into which it is directed, the only radiative properties of the stratosphere needed for climate modeling purposes are: 1) albedo for collimated radiation from above $\hat{R}(\tau_i, \mu_0)$; 2) albedo for diffuse radiation from below $\bar{R}^*(\tau_i)$; 3) transmission for collimated radiation from above, $\hat{T}(\tau_i, \mu_0)$ and $D(\tau_i, \mu_0)$; and 4) transmission for diffuse radiation from below, $\bar{T}^*(\tau_i)$ and $\bar{D}(\tau_i)$. The wavelength averaged values of these functions for each wavelength interval and for each microphysical model are parameterized and discussed in Section 4.

b. Longwave radiation

Although the stratospheric aerosol layer has a very small optical thickness at infrared wavelengths (cf. Fig. 3), the longwave screening effect of the layer is important in estimating the total radiative impact of the layer on the earth–atmosphere system. The basic quantities required as input to infrared radiative transfer models are the monochromatic transmission and reflection functions of the layer. For a purely absorbing medium, the reflection and diffuse transmission are zero, so that the total global transmission includes only the direct term, which is given by $2E_3(\tau_i)$, as in (12).

Since the El Chichon stratospheric aerosol layer has a small optical thickness at infrared wavelengths, the radiative properties of the aerosol layer may be obtained from the single scattering approximation. Noting that the aerosol asymmetry factor is small, it can be shown after some algebraic manipulation that

$$\bar{R}^*(\tau_i) = \omega_{0i}[G_{22}(\tau_i) - 3\langle\cos\Theta_i\rangle G_{33}(\tau_i)], \quad (14)$$

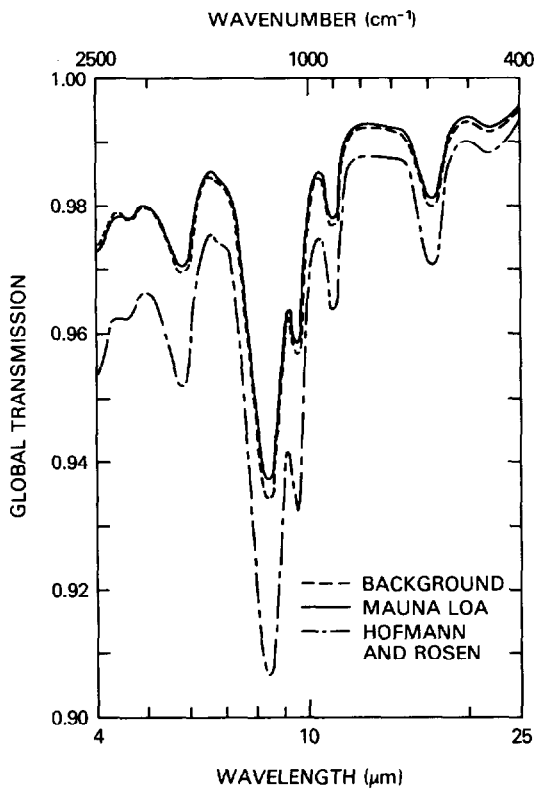

FIG. 10. Global transmission $\bar{T}^*(\tau_i) + \bar{D}(\tau_i)$ as a function of wavelength for $\lambda \geq 4.0$ μm and for the three stratospheric aerosol size distributions presented in Fig. 2. The transmission was obtained from (19) using the spectral optical thickness, single scattering albedo and asymmetry factor presented in Figs. 3–5.

$$\bar{T}^*(\tau_i) = \omega_{0i}[G'_{22}(\tau_i) + 3\langle\cos\Theta_i\rangle G'_{33}(\tau_i)], \quad (15)$$

where ω_{0i} and $\langle\cos\Theta_i\rangle$ are, respectively, the monochromatic values of the single scattering albedo and asymmetry factor, and $G_{nm}(\tau_i)$ and $G'_{nm}(\tau_i)$ are defined by (van de Hulst, 1980)

$$G_{nm}(x) = \int_0^x E_n(t)E_m(t)dt,$$

$$G'_{nm}(x) = \int_0^x E_n(t)E_m(x-t)dt.$$

Expanding the G functions for small values of τ_i, and neglecting terms of order $\tau_i^2 \ln\tau_i$ and terms of order τ_i^2 and higher, these expressions can be shown to reduce to the forms

$$\bar{R}^*(\tau_i) = \omega_{0i}(1 - 0.75\langle\cos\Theta_i\rangle)\tau_i, \quad (16)$$

$$\bar{T}^*(\tau_i) = \omega_{0i}(1 + 0.75\langle\cos\Theta_i\rangle)\tau_i, \quad (17)$$

$$\bar{A}^*(\tau_i) = 2(1 - \omega_{0i})\tau_i. \quad (18)$$

It follows from these results that the effects of scattering can be included in infrared radiative transfer models by replacing the aerosol optical thickness by an effective optical thickness such that the total global transmission of the aerosol layer for diffuse radiation may be written as

$$\bar{T}^*(\tau_i) + \bar{D}(\tau_i) = 2E_3\{[1 - 0.5\omega_{0i}(1 + 0.75\langle\cos\Theta_i\rangle)]\tau_i\}. \quad (19)$$

In applying these equations to infrared radiative transfer models, it is necessary to modify the transmission of any layer that contains aerosol particles. This may be accomplished by multiplying the transmission of the aerosol layer by that of the other optically active gases. In the relevant region of the infrared spectrum, where both ω_{0i} and $\langle\cos\Theta_i\rangle$ are ≤ 0.2 (cf. Figs. 4 and 5), the effective optical thickness is $\simeq\tau_i$ such that the total global transmission reduces to $2E_3(\tau_i)$. This allows us to largely neglect the effects of scattering for longwave radiation.

As an example, Fig. 10 illustrates the total global transmission of the aerosol layer as a function of wavelength for $\lambda \geq 4.0$ μm and for each of the

TABLE 2. The quadratic polynomial coefficients required to evaluate $\hat{R}_k(\tau_{ref}, \phi)$, $\hat{T}_k(\tau_{ref}, \phi)$ and $A_k(\tau_{ref}, \phi)$ according to Eqs. (20)–(22) for $\lambda \leq 0.83$ μm and for each of the three aerosol models.

Latitude (°N)	$a_1(\phi)$	$b_1(\phi)$	$c_1(\phi)$	$d_1(\phi)$	$e_1(\phi)$	$f_1(\phi)$	$g_1(\phi)$
				Background			
85	1.0158	−0.9734	2.3015	−3.3839	0.09002	−0.02196	−0.03297
75	0.9244	−0.8173	2.2126	−3.1383	0.08673	−0.01378	−0.04128
65	0.7391	−0.5284	2.0294	−2.6510	0.07774	0.00228	−0.05067
55	0.5261	−0.2487	1.7918	−2.0725	0.06801	0.01263	−0.04766
45	0.3867	−0.1045	1.6118	−1.6743	0.06082	0.01504	−0.03806
35	0.3002	−0.0351	1.4852	−1.4146	0.05449	0.01445	−0.02792
25	0.2488	−0.0032	1.4010	−1.2517	0.04967	0.01298	−0.02039
15	0.2200	0.0112	1.3509	−1.1579	0.04591	0.01154	−0.01499
5	0.2066	0.0169	1.3228	−1.1086	0.04536	0.01107	−0.01385
				Mauna Loa			
85	0.8237	−0.6314	2.2342	−3.0162	0.09002	−0.00656	−0.06577
75	0.7428	−0.5115	2.1450	−2.7843	0.08673	−0.00044	−0.06799
65	0.5824	−0.2995	1.9604	−2.3265	0.07774	0.01025	−0.06405
55	0.4053	−0.1129	1.7189	−1.7851	0.06801	0.01506	−0.04896
45	0.2948	−0.0298	1.5342	−1.4147	0.06082	0.01433	−0.03409
35	0.2289	0.0037	1.4036	−1.1751	0.05449	0.01214	−0.02259
25	0.1908	0.0164	1.3165	−1.0263	0.04967	0.01010	−0.01543
15	0.1697	0.0210	1.2643	−0.9408	0.04591	0.00857	−0.01100
5	0.1600	0.0225	1.2358	−0.8970	0.04536	0.00814	−0.01005
				Hofmann and Rosen (1983b)			
85	0.8511	−0.6599	2.3050	−3.1871	0.09002	−0.00904	−0.06246
75	0.7708	−0.5412	2.2106	−2.9379	0.08673	−0.00297	−0.06437
65	0.6114	−0.3305	2.0153	−2.4458	0.07774	0.00796	−0.06065
55	0.4339	−0.1414	1.7612	−1.8677	0.06801	0.01350	−0.04712
45	0.3212	−0.0525	1.5689	−1.4768	0.06082	0.01357	−0.03392
35	0.2526	−0.0132	1.4342	−1.2265	0.05449	0.01199	−0.02347
25	0.2123	0.0036	1.3450	−1.0722	0.04967	0.01028	−0.01671
15	0.1897	0.0108	1.2919	−0.9839	0.04591	0.00892	−0.01238
5	0.1793	0.0134	1.2628	−0.9388	0.04536	0.00850	−0.01143

microphysical models. The reduced transmission of the Hofmann and Rosen (1983b) model is due to the larger infrared optical thickness, although the effect is reduced somewhat by the relatively large values of the single scattering albedo and asymmetry factor. It is clear from Fig. 10 that the largest infrared screening effect is confined to the region $7 \leqslant \lambda \leqslant 10$ μm. The wavelength averaged values of the global transmission for each of 17 bands and for each aerosol model are parameterized and discussed in the following section.

4. Parameterization

a. Shortwave radiation

Wavelength averaged values of the diffuse reflection (albedo), diffuse transmission and fractional absorption for collimated radiation from above the stratosphere, presented in Figs. 7–9, have been fit to quadratics of the form

$$\hat{R}_k(\tau_{\text{ref}}, \phi) = a_k(\phi)\tau_{\text{ref}} + b_k(\phi)\tau_{\text{ref}}^2, \quad (20)$$

$$\hat{T}_k(\tau_{\text{ref}}, \phi) = c_k(\phi)\tau_{\text{ref}} + d_k(\phi)\tau_{\text{ref}}^2, \quad (21)$$

$$A_k(\tau_{\text{ref}}, \phi) = e_k(\phi) + f_k(\phi)\tau_{\text{ref}} + g_k(\phi)\tau_{\text{ref}}^2, \quad (22)$$

where $k = 1$ refers to $\lambda \leqslant 0.83$ μm and $k = 2$ to $\lambda > 0.83$ μm. The coefficients thus obtained for each microphysical model and for each latitude zone are presented in Table 2 for $\lambda \leqslant 0.83$ μm and Table 4 for $\lambda > 0.83$ μm. The fraction of direct radiation transmitted through the stratosphere may be obtained from the expression

$$D_k(\tau_{\text{ref}}, \phi) = 1 - \hat{R}_k(\tau_{\text{ref}}, \phi) - \hat{T}_k(\tau_{\text{ref}}, \phi) - A_k(\tau_{\text{ref}}, \phi). \quad (23)$$

The origin of the coefficient $e_k(\phi)$ arises from ozone absorption, and thus $e_2(\phi)$ must equal zero. Since the wavelength region $\lambda \leqslant 0.83$ μm contains 58% of the incident solar radiation, the total shortwave absorption in the absence of the aerosol layer is given by $0.58e_1(\phi)$. We compared these results to the ozone absorption parameterization of Lacis and Hansen (1974) and found, in general, that our values of shortwave absorption exceed their values by approximately 9%. This is undoubtedly due to differences

TABLE 3. The quadratic polynomial coefficients required to evaluate $\bar{R}_k^{\uparrow}(\tau_{\text{ref}}, \phi)$, $\bar{T}_k^{\downarrow}(\tau_{\text{ref}}, \phi)$ and $\bar{A}_k^{\downarrow}(\tau_{\text{ref}}, \phi)$ according to Eqs. (24)–(26) for $\lambda \leqslant 0.83$ μm and for each of the three aerosol models.

Latitude (°N)	$\bar{a}^{\uparrow}(\phi)$	$\bar{b}^{\uparrow}(\phi)$	$\bar{c}^{\downarrow}(\phi)$	$\bar{d}^{\downarrow}(\phi)$	$\bar{e}^{\downarrow}(\phi)$	$\bar{f}^{\downarrow}(\phi)$	$\bar{g}^{\downarrow}(\phi)$
			Background				
85	0.3112	−0.2202	1.3545	−1.3604	0.06031	0.01279	−0.01628
75	0.3112	−0.2202	1.3545	−1.3604	0.06031	0.01279	−0.01628
65	0.3135	−0.2232	1.3573	−1.3641	0.05884	0.01153	−0.01458
55	0.3158	−0.2262	1.3600	−1.3678	0.05743	0.01015	−0.01273
45	0.3183	−0.2295	1.3630	−1.3717	0.05592	0.00876	−0.01083
35	0.3225	−0.2352	1.3682	−1.3788	0.05328	0.00631	−0.00739
25	0.3271	−0.2414	1.3736	−1.3863	0.05055	0.00356	−0.00347
15	0.3322	−0.2483	1.3791	−1.3940	0.04781	0.00031	0.00124
5	0.3322	−0.2483	1.3791	−1.3940	0.04781	0.00031	0.00124
			Mauna Loa				
85	0.2570	−0.1667	1.2768	−1.1652	0.06031	0.01069	−0.01557
75	0.2570	−0.1667	1.2768	−1.1652	0.06031	0.01069	−0.01557
65	0.2590	−0.1693	1.2794	−1.1686	0.05884	0.00958	−0.01407
55	0.2610	−0.1720	1.2819	−1.1718	0.05743	0.00836	−0.01241
45	0.2632	−0.1749	1.2845	−1.1753	0.05592	0.00712	−0.01068
35	0.2668	−0.1798	1.2892	−1.1815	0.05328	0.00498	−0.00766
25	0.2708	−0.1852	1.2941	−1.1879	0.05055	0.00258	−0.00418
15	0.2751	−0.1911	1.2990	−1.1944	0.04781	−0.00020	−0.00012
5	0.2751	−0.1911	1.2990	−1.1944	0.04781	−0.00020	−0.00012
			Hofmann and Rosen (1983b)				
85	0.2738	−0.1766	1.3089	−1.2239	0.06031	0.01082	−0.01615
75	0.2738	−0.1766	1.3089	−1.2239	0.06031	0.01082	−0.01615
65	0.2758	−0.1792	1.3115	−1.2274	0.05884	0.00968	−0.01464
55	0.2779	−0.1819	1.3141	−1.2307	0.05743	0.00843	−0.01297
45	0.2801	−0.1848	1.3168	−1.2344	0.05592	0.00717	−0.01123
35	0.2839	−0.1898	1.3217	−1.2408	0.05328	0.00497	−0.00818
25	0.2879	−0.1952	1.3267	−1.2475	0.05055	0.00253	−0.00471
15	0.2923	−0.2012	1.3318	−1.2543	0.04781	−0.00031	−0.00061
5	0.2923	−0.2012	1.3318	−1.2543	0.04781	−0.00031	−0.00061

in the ozone absorption coefficients used in each investigation. A difference of this magnitude warrants further investigation since Lacis and Hansen's parameterization is widely used in global climate models.

Wavelength averaged values of the spherical albedo, global diffuse transmission and global absorption for diffuse radiation from below the stratosphere have similarly been parameterized in terms of quadratics of the form

$$\bar{R}_k^*(\tau_{\text{ref}}, \phi) = \bar{a}_k^*(\phi)\tau_{\text{ref}} + \bar{b}_k^*(\phi)\tau_{\text{ref}}^2, \quad (24)$$

$$\bar{T}_k^*(\tau_{\text{ref}}, \phi) = \bar{c}_k^*(\phi)\tau_{\text{ref}} + \bar{d}_k^*(\phi)\tau_{\text{ref}}^2, \quad (25)$$

$$\bar{A}_k^*(\tau_{\text{ref}}, \phi) = \bar{e}_k^*(\phi) + \bar{f}_k^*(\phi)\tau_{\text{ref}} + \bar{g}_k^*(\phi)\tau_{\text{ref}}^2. \quad (26)$$

The resulting coefficients for $\lambda \leq 0.83$ μm are presented in Table 3 for each microphysical model and for each latitude zone. The latitudinal variation of the coefficients arises entirely from the latitudinal variation of Ω_1 and Ω_2. Since the region $\lambda > 0.83$ μm is unaffected by ozone absorption, the coefficients for $k = 2$ show no latitudinal variation and are presented in Table 4 without reference to latitude. The global direct transmission follows from these results and is given by

$$\bar{D}_k(\tau_{\text{ref}}, \phi) = 1 - \bar{R}_k^*(\tau_{\text{ref}}, \phi) - \bar{T}_k^*(\tau_{\text{ref}}, \phi) - \bar{A}_k^*(\tau_{\text{ref}}, \phi). \quad (27)$$

b. Longwave radiation

For computing the band-averaged global transmission of the aerosol layer, the infrared spectrum was divided into 17 intervals between 4.55 and 25.0 μm. For each wavelength interval and aerosol model the

TABLE 4. The quadratic polynomial coefficients required to evaluate $\hat{R}_k(\tau_{\text{ref}}, \phi)$, $\hat{T}_k(\tau_{\text{ref}}, \phi)$ and $A_k(\tau_{\text{ref}}, \phi)$ according to Eqs. (20)–(22) for $\lambda > 0.83$ μm and for each of the three aerosol models. The coefficients for diffuse illumination from below the stratosphere are also presented.

Latitude (°N)	$a_2(\phi)$	$b_2(\phi)$	$c_2(\phi)$	$d_2(\phi)$	$e_2(\phi)$	$f_2(\phi)$	$g_2(\phi)$
				Background			
85	0.2755	−0.1040	0.4748	−0.2447	0.0	1.241×10^{-2}	-7.324×10^{-4}
75	0.2528	−0.0879	0.4514	−0.2216	0.0	1.164×10^{-2}	-6.338×10^{-4}
65	0.2073	−0.0590	0.4041	−0.1779	0.0	1.009×10^{-2}	-4.570×10^{-4}
55	0.1546	−0.0313	0.3478	−0.1316	0.0	8.281×10^{-3}	-2.868×10^{-4}
45	0.1191	−0.0163	0.3082	−0.1031	0.0	7.038×10^{-3}	-1.927×10^{-4}
35	0.0962	−0.0085	0.2813	−0.0855	0.0	6.215×10^{-3}	-1.411×10^{-4}
25	0.0821	−0.0046	0.2638	−0.0748	0.0	5.693×10^{-3}	-1.127×10^{-4}
15	0.0741	−0.0026	0.2531	−0.0687	0.0	5.386×10^{-3}	-9.761×10^{-5}
5	0.0701	−0.0016	0.2480	−0.0659	0.0	5.235×10^{-3}	-9.087×10^{-5}
Diffuse	0.1037	−0.0417	0.2752	−0.1122	0.0	6.359×10^{-3}	-5.288×10^{-4}
				Mauna Loa			
85	0.4087	−0.2153	0.8149	−0.6187	0.0	1.223×10^{-2}	-6.638×10^{-4}
75	0.3719	−0.1794	0.7775	−0.5642	0.0	1.148×10^{-2}	-5.625×10^{-4}
65	0.2996	−0.1174	0.6998	−0.4572	0.0	9.950×10^{-3}	-3.835×10^{-4}
55	0.2152	−0.0554	0.6074	−0.3442	0.0	8.166×10^{-3}	-2.161×10^{-4}
45	0.1599	−0.0261	0.5404	−0.2690	0.0	6.940×10^{-3}	-1.277×10^{-4}
35	0.1236	−0.0065	0.4954	−0.2270	0.0	6.128×10^{-3}	-8.151×10^{-5}
25	0.1026	0.0000	0.4647	−0.1979	0.0	5.614×10^{-3}	-5.736×10^{-5}
15	0.0896	0.0065	0.4472	−0.1846	0.0	5.310×10^{-3}	-4.508×10^{-5}
5	0.0840	0.0065	0.4379	−0.1751	0.0	5.162×10^{-3}	-3.955×10^{-5}
Diffuse	0.1393	−0.0750	0.4747	−0.2643	0.0	6.268×10^{-3}	-5.016×10^{-5}
				Hofmann and Rosen (1983b)			
85	0.5506	−0.3306	1.3395	−1.3321	0.0	1.992×10^{-2}	-1.553×10^{-3}
75	0.4982	−0.2711	1.2791	−1.2176	0.0	1.869×10^{-2}	-1.258×10^{-3}
65	0.3947	−0.1664	1.1537	−0.9934	0.0	1.620×10^{-2}	-7.515×10^{-4}
55	0.2791	−0.0726	0.9979	−0.7422	0.0	1.329×10^{-2}	-3.093×10^{-4}
45	0.2053	−0.0281	0.8831	−0.5778	0.0	1.129×10^{-2}	-1.021×10^{-4}
35	0.1599	−0.0078	0.8029	−0.4740	0.0	9.969×10^{-3}	-1.048×10^{-5}
25	0.1329	0.0014	0.7499	−0.4107	0.0	9.130×10^{-3}	2.896×10^{-5}
15	0.1178	0.0055	0.7178	−0.3744	0.0	8.635×10^{-3}	4.553×10^{-5}
5	0.1107	0.0071	0.7018	−0.3570	0.0	8.393×10^{-3}	5.173×10^{-5}
Diffuse	0.1880	−0.1166	0.7576	−0.5285	0.0	1.015×10^{-2}	-1.114×10^{-3}

TABLE 5. The linear coefficients required to evaluate the global transmission at 220 K for 17 infrared bands and for each of the three aerosol models.

Band center (μm)	Wavenumber interval (cm^{-1})	$\bar{h}_k$ Background	$\bar{h}_k$ Mauna Loa	$\bar{h}_k$ Hofmann and Rosen
4.71	2050–2200	0.08406	0.08443	0.14467
5.00	1950–2050	0.08236	0.08127	0.13764
5.26	1850–1950	0.09327	0.09090	0.14951
5.56	1750–1850	0.11560	0.11224	0.18047
5.88	1650–1750	0.11396	0.11102	0.18204
6.25	1550–1650	0.07204	0.07057	0.11967
6.67	1450–1550	0.06393	0.06153	0.10103
7.14	1350–1450	0.08445	0.08022	0.12412
7.84	1200–1350	0.20833	0.19595	0.28605
8.51	1150–1200	0.25600	0.24487	0.36961
9.09	1050–1150	0.17352	0.16741	0.26944
10.26	900–1050	0.08732	0.08428	0.14253
11.77	800–900	0.04868	0.04699	0.07915
13.16	720–800	0.02856	0.02702	0.04518
15.15	600–720	0.04482	0.04195	0.06622
18.18	500–600	0.04806	0.04552	0.07146
22.22	400–500	0.02830	0.02617	0.04123

monochromatic global transmission was weighted by the Planck function at temperatures between 200 and 280 K. For bands having narrow wavelength intervals, as in those presented in Table 5, the wavelength averaged values of the global transmission are primarily a function of aerosol optical thickness with a much smaller dependence on temperature. In this situation it is sufficiently accurate to parameterize the global transmission for each band (k) by an equation of the form

$$\bar{T}_k^*(\tau_{\text{ref}}) + \bar{D}_k(\tau_{\text{ref}}) = 1 - \bar{h}_k\tau_{\text{ref}}. \quad (28)$$

For wider wavelength intervals or for bands composed of noncontiguous regions, as in the model described by Peng *et al.* (1982), the coefficient $\bar{h}_k$ has a significant temperature dependence. In order to obtain the global transmission of the stratosphere for each wavelength interval, the transmission of the aerosol layer must be multiplied by that for ozone, water vapor and carbon dioxide, as appropriate.

Table 5 presents the coefficients $\bar{h}_k$ required to evaluate (28) at 220 K for each band and for each aerosol model. As expected from the monochromatic results presented in Fig. 10 (applicable for $\tau_{\text{ref}} = 0.2476$), the global transmission for the background model is virtually identical to that for the Mauna Loa model. The presence of the large particle mode in the Hofmann and Rosen (1983b) model results in a much larger infrared screening effect than in either of the other two microphysical models. Assuming the global transmission at wavenumbers less than 340 cm^{-1} is unity, the mean value of $\bar{h}_k$ at 220 K (260 K) for the entire infrared spectrum is 0.04176 (0.05462) for the background model, 0.03963 (0.05200) for the Mauna Loa model and 0.06324 (0.08280) for the Hofmann and Rosen (1983b) model.

5. Spatial and temporal distribution

The initial injection of material into the stratosphere from El Chichon was at a latitude of 17.3°N and a longitude of 93.2°W. The stratospheric aerosol layer spread very rapidly in a zonal direction circling the globe in less than a month (Robock and Matson, 1983). Meridional dispersion was, on the other hand, quite slow. McCormick and Swissler (1983) report, on the basis of a coordinated aircraft flight mission during late October and early November 1982, that the bulk of the aerosol particles from El Chichon was concentrated in a layer between 24 and 26 km in altitude that extended over latitudes from 5–7°S to 35–37°N. In addition to the airborne lidar measurements described by McCormick and Swissler (1983), Spinhirne (1983) obtained measurements of the spectral optical thickness as a function of latitude. These results suggest that the larger particles associated with the Mauna Loa and Hofmann and Rosen (1983b) microphysical models are principally applicable over latitudes from 30°N to at least 7°S. Information about the temporal decay of the aerosol layer at a single latitude is available for the first four months from Mauna Loa measurements of the aerosol optical thickness (DeLuisi *et al.*, 1983).

In order to estimate the impact of El Chichon on temperatures of the Northern and Southern Hemispheres, it is necessary to develop a spatial and temporal distribution model of the aerosol layer to accompany the radiative parameterizations presented in the previous section. For at least the first seven months following the eruptions of El Chichon, the aerosol layer was confined to tropical latitudes south of 35–37°N. Eventually, however, the aerosol is expected to diffuse into high latitudes of the Northern and Southern Hemispheres at the same time as the total mass loading of the atmosphere is decreasing. Assuming that the dominant processes governing aerosol dispersion are diffusive transport in latitude and exponential decay in time, it follows that $\tau_{\text{ref}}(\phi, t)$ must satisfy the equation

$$\frac{\partial \tau_{\text{ref}}(\phi, t)}{\partial t} = \frac{1}{\cos\phi}\frac{\partial}{\partial \phi}\left[\mathcal{D}\cos\phi\frac{\partial \tau_{\text{ref}}(\phi, t)}{\partial \phi}\right] - \frac{\tau_{\text{ref}}(\phi, t)}{\mathcal{T}} = \frac{\partial}{\partial x}\left[\mathcal{D}(1-x^2)\frac{\partial \tau_{\text{ref}}(\phi, t)}{\partial x}\right] - \frac{\tau_{\text{ref}}(\phi, t)}{\mathcal{T}}, \quad (29)$$

where $\mathcal{T}$ is the time constant, $\mathcal{D}$ the diffusion coefficient and $x = \sin\phi$. If we assume that the spatial and temporal distribution of aerosol optical thickness at 0.55 μm, $\tau_{ref}(\phi, t)$, is of the form

$$\tau_{ref}(\phi, t) = B(\phi, t) \exp(-t/\mathcal{T}),$$

and substitute this expression into (29), it follows that $B(\phi, t)$ must satisfy the equation

$$\frac{\partial B(\phi, t)}{\partial t} = \frac{\partial}{\partial x}\left[\mathcal{D}(1 - x^2)\frac{\partial B(\phi, t)}{\partial x}\right]. \quad (30)$$

If we make the simplification that $\mathcal{D}$ is a constant, independent of x, and further note that the Legendre polynomials are eigenfunctions of the diffusion operator,

$$\frac{d}{dx}\left[(1 - x^2)\frac{dP_l(x)}{dx}\right] = -l(l + 1)P_l(x), \quad (31)$$

it follows that the Legendre polynomials $P_l(x)$ form a convenient basis set for expanding $B(\phi, t)$. Therefore, expressing $B(\phi, t)$ as an expansion in Legendre polynomials of the form

$$B(\phi, t) = \sum_{l=0}^{\infty} B_l(t)P_l(x),$$

we find, on insertion into (30), that the solution for $\tau_{ref}(\phi, t)$ is given by

$$\tau_{ref}(\phi, t) = \sum_{l=0}^{\infty} B_l(0)P_l(x) \exp[-l(l + 1)\mathcal{D}t - t/\mathcal{T}]. \quad (32)$$

In order to evaluate the expansion coefficients $B_l(0)$, it is necessary to apply boundary conditions. We assume that at time $t = 0$, the optical thickness of the aerosol layer resulting from the El Chichon eruptions is confined to a latitude $\phi_0 = 17.3°$N such that

$$\tau_{ref}(\phi, 0) = 2\tau_0\delta(x - x_0), \quad (33)$$

where τ_0 is the global mean aerosol optical thickness at time $t = 0$, $\delta(x - x_0)$ is the Dirac delta function, and $x_0 = \sin\phi_0$. Noting that the delta function satisfies the Legendre polynomial expansion (Morse and Feshbach, 1953, p. 729),

$$\delta(x - x_0) = \sum_{l=0}^{\infty} \frac{1}{2}(2l + 1)P_l(x)P_l(x_0), \quad (34)$$

and substituting this expression into (32) and (33), it follows that the diffusion model for the spatial and temporal distribution of the aerosol layer is given by

$$\tau_{ref}(\phi, t) = \tau_0 \sum_{l=0}^{\infty} (2l + 1)P_l(x)P_l(x_0) \times \exp[-l(l + 1)\mathcal{D}t - t/\mathcal{T}]. \quad (35)$$

The diffusion model presented here, though still an oversimplification of the many microphysical and dynamical properties governing aerosol dispersion in the stratosphere, has the sought after property of an initial injection of aerosol at low latitudes, followed by latitudinal spreading and reduced mass loading with time. The global mean aerosol optical thickness at 0.55 μm, denoted $\bar{\tau}_{ref}(t)$, is given by

$$\bar{\tau}_{ref}(t) = \frac{1}{2}\int_{-1}^{1} \tau_{ref}(\phi, t)dx, = \tau_0 \exp(-t/\mathcal{T}). \quad (36)$$

For the diffusion model, the latitudinal distribution of aerosol optical thickness contains modes of various spatial scales, but the higher order modes decay with shorter time constants than the global scale mode ($l = 0$).

The adjustable parameters in the diffusion model are the initial global mean aerosol optical thickness τ_0, the time constant $\mathcal{T}$ and the diffusion coefficient $\mathcal{D}$. Various data sets can be used to estimate values of τ_0, $\mathcal{T}$ and $\mathcal{D}$ which best describe the evolution of the El Chichon eruption cloud. Swissler *et al.* (1983) have presented the latitudinal distribution of aerosol optical thickness obtained by using an optical model to convert monostatic lidar measurements to optical thickness. The lidar observations, which were obtained during the airborne latitudinal survey described by McCormick and Swissler (1983), covered the latitude region between 46°N and 46°S from 19 October to 7 November 1982. The results of Swissler *et al.* (1983) for the southbound portion of the flights were fit to (35) using an efficient gradient-expansion method from nonlinear least-squares theory (Bevington, 1969). The diffusion model coefficients yielding the best fit to these data for $t = 7$ months were $\tau_0 = 0.144$, $\mathcal{D} = 0.01774$ mo^{-1} and $\mathcal{T} = 10.03$ mo. The latitudinal distribution of optical depth after seven months for the diffusion model is compared in Fig. 11 with the Swissler *et al.* (1983) observations. Though Swissler *et al.* results apply to a wavelength of 0.6943 μm, corresponding to the wavelength of their ruby lidar system, little difference is expected between the optical depth at 0.55 μm and that at 0.6943 μm (cf. Fig. 3).

In the diffusion model the aerosol layer starts out confined to low latitudes, eventually spreading uniformly over the globe. The latitude of peak optical depth slowly moves from the latitude of injection (in this case $\phi_0 = 17.3°$N) toward the pole of the hemisphere of injection. During the early months

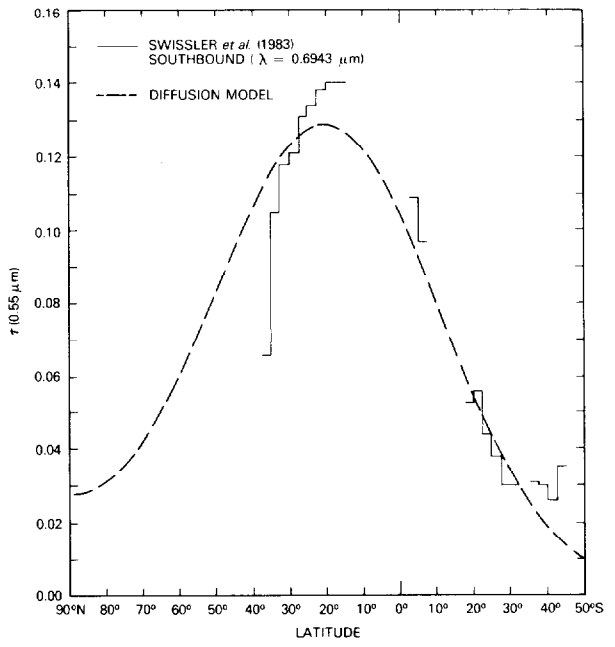

FIG. 11. The latitudinal distribution of aerosol optical thickness at 0.55 μm seven months following the eruptions of El Chichon for the diffusion model described in the text, where $\tau_0 = 0.144$, $\mathcal{T} = 10.03$ months (mo) and $\mathcal{D} = 0.01774$ mo^{-1} (dashed curve). The solid curve corresponds to the aerosol optical thickness derived from monostatic lidar measurements at 0.6943 μm (after Swissler *et al.*, 1983).

following the eruptions and for small values of $\mathcal{D}$, our diffusion model is similar to the empirical expression used by Robock (1981), where Robock used the numerical model of Cadle *et al.* (1976) to fit a diffusion-type equation in one dimension. In Robock's model the peak aerosol optical depth remains fixed at the latitude of injection.

In order to account for the evolution of the aerosol size distribution from post-volcanic conditions to background conditions as the aerosol layer evolves in space and time, we assume that the albedo of the aerosol layer $\hat{R}_k(\tau_{\text{ref}}, \phi)$ may be expressed as

$$\hat{R}_k(\tau_{\text{ref}}, \phi) = \hat{R}_k^{\text{EC}}(\tau_{\text{ref}}, \phi) \exp(-t/\mathcal{T}) + \hat{R}_k^{\text{BK}}(\tau_{\text{ref}}, \phi)[1 - \exp(-t/\mathcal{T})]. \quad (37)$$

In this expression $\hat{R}_k^{\text{EC}}(\tau_{\text{ref}}, \phi)$ is the albedo for either of the two El Chichon models [Mauna Loa or Hofmann and Rosen (1983b)] and $\hat{R}_k^{\text{BK}}(\tau_{\text{ref}}, \phi)$ the albedo for the background model. In this way it is possible for the albedo of the aerosol layer to closely resemble that for post-volcanic conditions during the early months and background conditions during the later months following volcanic eruptions. Similar expressions apply to the other radiative properties of the stratospheric layer [viz., $\hat{T}_k(\tau_{\text{ref}}, \phi)$, $A_k(\tau_{\text{ref}}, \phi)$, $\bar{R}_k^*(\tau_{\text{ref}}, \phi)$, $\bar{T}_k^*(\tau_{\text{ref}}, \phi)$ and $\bar{A}_k^*(\tau_{\text{ref}}, \phi)$].

6. Summary and conclusions

The present study has examined the effect of the El Chichon stratospheric aerosol layer on radiation reflected, transmitted and absorbed by the stratosphere. The optical thickness, single scattering albedo and asymmetry factor of the aerosol particles were obtained as a function of wavelength between 0.25 and 25.0 μm for three models of the statospheric aerosol size distribution. These results, presented in Figs. 3–5, are based on the assumption that the aerosol layer is composed of spherical droplets having a 75% (by weight) H_2SO_4 aqueous solution. Two of the size distribution models were derived from measurements of the El Chichon aerosol layer while the third model is representative of a stratospheric aerosol layer unperturbed by recent volcanic activity. For the shortwave spectral region, multiple-scattering computations of the diffuse reflection (albedo), diffuse transmission and fractional absorption were obtained using successive applications of the invariant imbedding and doubling methods where polarization has been neglected. These results, presented in Figs. 7–9 and parameterized in Tables 2–4, were obtained for each of two wavelength intervals as a function of latitude, optical thickness and aerosol size distribution. For the longwave region, the global transmission (flux transmissivity) is presented and parameterized for 17 wavelength intervals using the single scattering approximation to account for the small, scattering component of the aerosols at infrared wavelengths.

In addition to the optical and radiative properties of the stratospheric aerosol layer, a simple model of the spatial and temporal distribution of aerosol optical thickness is developed. This model is based on the simplifying assumption that the dominant processes governing aerosol dispersion in the stratosphere are diffusive transport in latitude and exponential decay in time. The three adjustable parameters in the diffusion model are the time constant, diffusion coefficient and initial global mean aerosol optical thickness at 0.55 μm. They are determined by a best fit to the latitudinal distribution of aerosol optical thickness derived from monostatic lidar measurements during an airborne latitudinal survey from late October to early November 1982.

As the aerosol layer evolves in space and time, the aerosol size distribution is expected to evolve from post-volcanic conditions to background conditions. In order to account for this evolution in the aerosol size distribution, we introduce a simple means by which the radiative properties of one of the two El Chichon models can be combined with the radiative properties of the background model to yield a realistic estimate of the radiative properties during time varying conditions. For low latitudes close to the latitude of El Chichon, the aerosol optical thickness is initially

large and the size distribution close to one of the two El Chichon microphysical models. As the optical thickness decays with time at these latitudes, the radiative properties would slowly change, both as a result of a changing optical thickness and as a result of a changing microphysical model. At higher latitudes, where the optical thickness is initially small, the optical thickness would initially increase with the radiative properties following the expectations of one of the two El Chichon models. Eventually, as the optical thickness begins to decrease, the radiative properties would more closely follow the expectations of the background microphysical model.

The parameterizations presented in this paper for solar and infrared radiation, together with the dispersion model and the relationship for varying the size distribution with time, permit climate models to realistically evaluate the impact of El Chichon on temperatures of the Northern and Southern Hemispheres. Our radiative parameterizations are especially well suited to annually and zonally averaged models such as the multi-layer energy balance model described by Peng *et al.* (1982). Results obtained using this climate model will be reported separately.

A significant finding of the present investigation is the importance of the 1.0 μm mode of the El Chichon aerosol size distribution reported by Hofmann and Rosen (1983b). The presence of these particles is largely responsible for the differences in the optical and radiative properties between the Mauna Loa and Hofmann and Rosen aerosol models, especially in the near- and thermal-infrared regions. As a consequence of the importance of these particles on the radiative properties of the stratosphere, the need to measure the particle concentration out to radii of $\sim$2.0 μm for future volcanic eruptions cannot be overemphasized. The spectral optical thickness measurements at Mauna Loa Observatory, being restricted to wavelengths $\leq$ 1.06 μm, do not permit an accurate determination of the particle concentration at radii much greater than 1.0 μm. The fact that the optical thickness at 1.06 μm was substantially lower than at 0.86 μm (cf. Figs. 2 and 3) suggests that the 1.0 μm mode, if present, was not significant at Mauna Loa during July 1982.

Acknowledgments. The authors are grateful to Howard G. Meyer for aid in performing the computations. This research was in part supported by funding provided by NASA Grant NAG 5-309.

REFERENCES

Ackerman, M., 1971: Ultraviolet solar radiation related to mesospheric processes. *Mesospheric Models and Related Experiments,* G. Fiocco, Ed., D. Reidel, 149–159.

Bevington, P. R., 1969: *Data Reduction and Error Analysis for the Physical Sciences.* McGraw-Hill, 336 pp.

Cadle, R. D., C. S. Kiang and J. F. Louis, 1976: The global scale dispersion of the eruption clouds from major volcanic eruptions. *J. Geophys. Res.,* **81,** 3125–3132.

Coulson, K. L., 1983: Effects of the El Chichon volcanic cloud in the stratosphere on the polarization of light from the sky. *Appl. Opt.,* **22,** 1036–1050.

DeLuisi, J. J., E. G. Dutton, K. L. Coulson, T. E. DeFoor and B. G. Mendonca, 1983: On some radiative features of the El Chichon volcanic stratospheric dust cloud and a cloud of unknown origin observed at Mauna Loa. *J. Geophys. Res.,* **88,** 6769–6772.

Hansen, J. E., and L. D. Travis, 1974: Light scattering in planetary atmospheres. *Space Sci. Rev.,* **16,** 527–610.

Harshvardhan, 1979: Perturbation of the zonal radiation balance by a stratospheric aerosol layer. *J. Atmos. Sci.,* **36,** 1274–1285.

——, and R. D. Cess, 1976: Stratospheric aerosols: Effect upon atmospheric temperature and global climate. *Tellus,* **28,** 1–10.

Herman, B. M., S. R. Browning and R. Rabinoff, 1976: The change in earth–atmosphere albedo and radiational equilibrium temperatures due to stratospheric pollution. *J. Appl. Meteor.,* **15,** 1057–1067.

Hofmann, D. J., and J. M. Rosen, 1982: Balloon-borne observations of stratospheric aerosol and condensation nuclei during the year following the Mt. St. Helens eruption. *J. Geophys. Res.,* **87,** 11 039–11 061.

——, and ——, 1983a: Stratospheric sulfuric acid fraction and mass estimate for the 1982 volcanic eruption of El Chichon. *Geophys. Res. Lett.,* **10,** 313–316.

——, and ——, 1983b: Sulfuric acid droplet formation and growth in the stratosphere after the 1982 eruption of El Chichon. *Science,* **222,** 325–327.

Inn, E. C. Y., and Y. Tanaka, 1953: Absorption coefficient of ozone in the ultraviolet and visible regions. *J. Opt. Soc. Amer.,* **43,** 870–873.

King, M. D., 1982: Sensitivity of constrained linear inversions to the selection of the Lagrange multiplier. *J. Atmos. Sci.,* **39,** 1356–1369.

——, 1983: Number of terms required in the Fourier expansion of the reflection function for optically thick atmospheres. *J. Quant. Spectrosc. Radiat. Transfer,* **30,** 143–161.

——, D. M. Byrne, B. M. Herman and J. A. Reagan, 1978: Aerosol size distributions obtained by inversion of spectral optical depth measurements. *J. Atmos. Sci.,* **35,** 2153–2167.

Krueger, A. J., 1983: Sighting of El Chichon sulfur dioxide clouds with the Nimbus 7 total ozone mapping spectrometer. *Science,* **220,** 1377–1379.

Lacis, A. A., and J. E. Hansen, 1974: A parameterization for the absorption of solar radiation in the earth's atmosphere. *J. Atmos. Sci.,* **31,** 118–133.

Lenoble, J., D. Tanre, P. Y. Deschamps and M. Herman, 1982: A simple method to compute the change in earth–atmosphere radiative balance due to a stratospheric aerosol layer. *J. Atmos. Sci.,* **39,** 2565–2576.

McClatchey, R. A., H. J. Bolle and K. Ya. Kondratyev, 1980: Report of the IAMAP Radiation Commission working group on a Standard Radiation Atmosphere. WMO/IAMAP, 33 pp. [Available from AFGL, Hanscom Air Force Base, MA 01731.]

——, R. W. Fenn, J. E. A. Selby, F. E. Volz and J. S. Garing, 1972: Optical Properties of the Atmosphere, 3rd ed., Rep. AFCRL-72-0497, Air Force Cambridge Research Laboratories, 108 pp. [NTIS AD753075].

McCormick, M. P., and T. J. Swissler, 1983: Stratospheric aerosol mass and latitudinal distribution of the El Chichon eruption cloud for October 1982. *Geophys. Res. Lett.,* **10,** 877–880.

Mitchell, J. M., 1982: El Chichon: Weather-maker of the century? *Weatherwise,* **35,** 252–261.

Morse, P. M., and H. Feshbach, 1953: *Methods of Theoretical Physics, Part I.* McGraw-Hill, 997 pp.

Palmer, K. F., and D. Williams, 1975: Optical constants of sulfuric acid; application to the clouds of Venus? *Appl. Opt.*, **14,** 208–219.

Peng, L., M. D. Chou and A. Arking, 1982: Climate studies with a multi-layer energy balance model. Part I: Model description and sensitivity to the solar constant. *J. Atmos. Sci.*, **39,** 2639–2659.

Penny, C. M., 1979: Study of temperature dependence of the Chappuis band absorption of ozone. NASA CR-158977, General Electric Company, Schenectady, NY, 22 pp.

Pollack, J. B., O. B. Toon, C. Sagan, A. Summers, B. Baldwin and W. Van Camp, 1976: Volcanic explosions and climate change: A theoretical assessment. *J. Geophys. Res.*, **81,** 1071–1083.

Robock, A., 1981: A latitudinally dependent volcanic dust veil index, and its effect on climate simulations. *J. Volcanol. Geotherm. Res.*, **11,** 67–80.

——, and M. Matson, 1983: Circumglobal transport of the El Chichon volcanic dust cloud. *Science,* **221,** 195–197.

Rosen, J. M., 1971: The boiling point of stratospheric aerosols. *J. Appl. Meteor.*, **10,** 1044–1046.

Shaw, G. E., 1979: Aerosols at Mauna Loa: Optical properties. *J. Atmos. Sci.*, **36,** 862–869.

Spinhirne, J. D., 1983: El Chichon eruption cloud: Latitudinal variation of the spectral optical thickness for October 1982. *Geophys. Res. Lett.*, **10,** 881–884.

Swissler, T. J., M. P. McCormick and J. D. Spinhirne, 1983: El Chichon eruption cloud: Comparison of lidar and optical thickness measurements for October 1982. *Geophys. Res. Lett.*, **10,** 885–888.

Turco, R. P., R. C. Whitten and O. B. Toon, 1982: Stratospheric aerosols: Observation and theory. *Rev. Geophys. Space Phys.*, **20,** 233–279.

van de Hulst, H. C., 1980: *Multiple Light Scattering. Tables, Formulas, and Applications,* Vols. 1 and 2. Academic Press, 739 pp.

Vigroux, E., 1953: Contribution a l'etude experimentale de l'absorption de l'ozone. *Ann. Phys.*, **8,** 709–762.